Data in Brief 33 (2020) 106562

Contents lists available at ScienceDirect

Data in Brief

journal homepage: www.elsevier.com/locate/dib

Data Article

Data of interaction of supported ionic liquids phases onto copper nanoparticles: A density functional theory study

Kerry Wrighton-Araneda[a], Cristián Valdebenito[b], Gabriel Abarca[b,*], Diego Cortés-Arriagada[a,*]

[a] Programa Institucional de Fomento a la Investigación, Desarrollo e Innovación. Universidad Tecnológica Metropolitana, Ignacio Valdivieso 2409, P.O. Box, San Joaquín, Santiago 8940577, Chile
[b] Universidad Bernardo O'Higgins, Escuela de Obstetricia y Puericultura, Centro Integrativo de Biología y Química Aplicada (CIBQA), Santiago 8370993, Chile

ARTICLE INFO

Article history:
Received 30 July 2020
Revised 16 November 2020
Accepted 17 November 2020
Available online 23 November 2020

Keywords:
DFT calculations
Ionic liquids
Adsorption energy
Nanoparticles

ABSTRACT

This work contains data on the computational, structural, and electronic characterization of supported ionic liquids phases anchored to copper nanoparticles using Density Functional theory calculations. The data supplement the paper "Interaction of supported ionic liquids phases onto copper nanoparticles: A Density Functional Theory study" [1], based on the adsorption of ionic liquid onto a Cu nanoparticle is analyzed from a chemical and physical point of view. The chemical analysis is based on Atoms in Molecule theory (AIM) and allows us to differentiate the chemical binding nature between ionic liquid and copper nanoparticle. On the other hand, the energy decomposition analysis based on absolutely localized molecular orbital (ALMO-EDA) describes the physical contributions that govern the interaction between ionic liquid and the copper nanoparticles. Herein, detailed and extended information in the synthesis and computational characterization are presented.

DOI of original article: 10.1016/j.molliq.2020.113089
* Corresponding author.
E-mail addresses: gabriel.abarca@ubo.cl (G. Abarca), dcortes@utem.cl (D. Cortés-Arriagada).
https://doi.org/10.1016/j.dib.2020.106562

Specifications Table

Subject	Chemistry
Specific subject area	Physical and Theoretical chemistry
Type of data	Graph, Fig, and Image.
How data were acquired	Computational data was acquired using Density functional theory calculations for structures optimization. Adsorption energy was calculated using electronic energy. Thermodynamic parameters for the adsorption process were calculated from the vibrational analysis. Energy decomposition analysis was employed to determine physical contribution. The nature of chemical bonding was studied using Atom in Molecules analysis (AIM). Experimental data were acquired using X-ray photoelectron spectroscopy (XPS) measurements were performed using a Kratos AXIS Ultra DLD instrument. The chamber pressure during the measurements was 5×10^{-9} Torr. Wide energy range survey scans were collected at pass energy of 80 eV in hybrid slot lens mode and a step size of 0.5 eV. High-resolution data on the C 1 s, N 1 s, and F 1 s photoelectron peaks were collected at pass energy 20 eV over energy ranges suitable for each peak, and collection times of 5 min, step sizes of 0.1 eV. The charge neutralizer filament was used to prevent the sample from charging over the irradiated area. The X-ray source was a monochromated Al K_α emission, run at 10 mA and 12 kV (120 W). The energy range for each 'pass energy' (resolution) was calibrated using the Kratos Cu $2p_{3/2}$, Ag $3d_{5/2,}$ and Au $4f_{7/2}$ three-point calibration method. The data were charge corrected to the reference carbon adventitious signal at 284.8 eV X-ray photoelectron spectroscopy.
Data format	Raw data and analyzed
Parameters for data collection	Computational data: The DFT calculations were developed considering standard convergence criteria for self-consistent field and geometry optimization procedures. Experimental data: XPS measurements were carried out using a Kratos AXIS Ultra DLD instrument. High-resolution XPS data on the C 1 s, N 1 s, and F 1 s photoelectron peaks were collected at pass energy 20 eV over energy ranges suitable for each peak, collection times of 5 min, and step sizes of 0.1 eV.
Description of data collection	Computational data: the data were collected from DFT calculations using visualization tools as VIM, Geany, and Chemcraft programs. Further wavefunction analyses were developed using the Multiwfn3.6 program. Experimental data: XPS provided insight into the interactions between surface Cu NP and the ionic liquids. The transmission function was calibrated using a clean gold sample method for all lens modes and the Kratos transmission generator software within Vision II. The data were processed with CASAXPS (Version 2.3.17).
Data source location	Computational Data: Programa Institucional de Fomento a la Investigación, Desarrollo e Innovación. Universidad Tecnológica Metropolitana. Ignacio Valdivieso 2409, P.O. Box 8,940,577, San Joaquín, Santiago, Chile. Experimental Data: Universidad Bernardo O'Higgins, Escuela de Obstetricia y Puericultura, Centro Integrativo de Biología y Química Aplicada (CIBQA), Santiago, 8,370,993, Chile.
Data accessibility	Data are available within this article Repository name: Mendeley Data Data identification number: 1 Direct URL to data: http://dx.doi.org/10.17632/zr3vf3bxpk.1 https://data.mendeley.com/datasets/zr3vf3bxpk/1 DOI:10.17632/zr3vf3bxpk.1
Related research article	*K. Wrighton-Araneda, C. Valdebenito, M.B. Camarada, G. Abarca, D. Cortés-Arriagada. Interaction of supported ionic liquids phases onto copper nanoparticles: A DFT study. Journal of Molecular Liquids 310 (2020) 113,089.* DOI:10.1016/j.molliq.2020.113089

Value of the Data

- The new Cu@(X)SILPs synthesized systems open a new route of triazolium based SILPs for catalysis and technological applications.
- The work explores the chemical and physical properties involved in the interaction of a new family of triazolium based SILP onto Cu NPs.
- The determination of the physical contributions involved in Cu@(X)SILPs complexes provide a deeper understanding of the stabilization and adsorption phenomena.

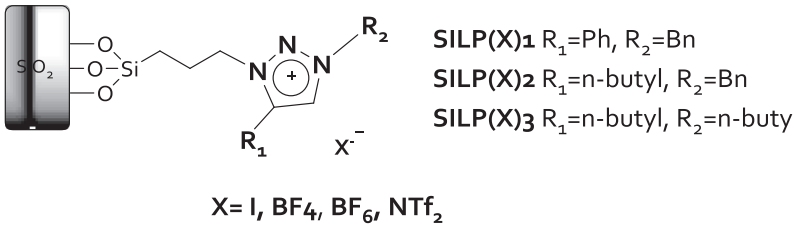

Fig. 1. Synthetic route for obtention of SILP(X)1–3. Modified from [1].

1. Data Description

For this work, we designed a series of new triazolium-based supported ionic liquids (SILPs), decorated with Cu NP (Cu@SILPs). The triazoles moieties were functionalized using copper-catalyzed azide-alkyne cycloaddition. Three triazolium cations ($T1^+$, $T2^+$, and $T3^+$) and four anions (I^-, BF_4^-, PF_6^-, and NTf_2^-) were considered to form the Cu@SILPs complexes. XPS and computational analysis gave mechanistic insights into the Cu NP stabilization pathways, where the anion adsorption onto Cu NP is favored compared to the cation adsorption. The stronger adsorption is observed for Cu@(I)SILP1 complex, which presents the more electron-rich triazole and the higher adsorption value of SILP onto Cu surface (5.18 eV). Computational studies of the adsorption of SILP onto Cu NPs allow evaluating the chemical and physical properties that govern these complexes stability. The schematic representation of Cu@(X)SILPs complexes is displayed in Fig 1.

The Cu@SILPs complexes stability was characterized by the adsorption energy (E_{ads}) (Eq. (1)), where the E_{Cu}, E_{cat}, E_{ani}, and $E_{Cu@SILP}$ correspond to the total energy of Cu_{55}, ionic liquid triazolium cation, ionic liquid anion, and the whole Cu@SILP systems. A more positive value of E_{ads} indicates a higher stabilization. The standard counterpoise method of *Boys* and *Bernardi* was implemented to correct the energy basis set superposition error (BSSE) [2].

From a physical viewpoint, the adsorption energy can be divided into two terms (Eq. (2)): preparation energy (ΔE_{PREP}) and interaction energy (ΔE_{INT}). The energy decomposition analysis based on absolutely localized molecular orbital (ALMO-EDA), implemented in Q-Chem 5.2 computational package [3,4], allows separating the adsorption energy into physically meaningful terms [5]. According to this scheme, the E_{ads} of a three-fragment A-B-C complex can be decomposed in their physical terms (Eq. (3)):

$$E_{ads} = E_{Cu} + E_{cat} + E_{ani} - E_{Cu@SILP} \tag{1}$$

$$-E_{ads} = \Delta E_{PREP} + \Delta E_{INT} \tag{2}$$

$$-E_{ads} = \Delta E_{PREP} + \Delta E_{POL} + \Delta E_{CT} + \Delta E_{ELEC} + \Delta E_{PAULI} + \Delta E_{DISP} \tag{3}$$

Where ΔE_{POL}, ΔE_{CT}, and ΔE_{ELEC} correspond to Polarization, Charge-Transfer, and Electrostatic energies as the stabilizing physical contributions, while ΔE_{PAULI} and ΔE_{PREP} energy are the destabilizing physical contributions. To verify ORCA consistency with Q-Chem5.2 (ALMO-EDA) calculations, the ΔE_{INT} was employed as a comparative case (Fig. 2). Due to the tendency and values calculated between both programs are consistent, further studies were performed. Fig. 2 displays the comparison between $\boldsymbol{\Delta E_{INT}}$ calculated using Q-chem and ORCA to validate both computational programs transferability.

The method to evaluate the interaction includes using two groups of system, the binary and ternary systems. Binary systems are formed by Cu NP bonded to an anion or cation, while ternary systems are formed by Cu NP, the anion, and the cation of the ionic liquid. The binary systems present a lower number of specific interactions, while ternary shows a full set of specific interactions. Therefore, the ΔE_{INT} of binary is less stabilized (Fig. 2). This methodology evaluates the stabilization as a process of successive steps.

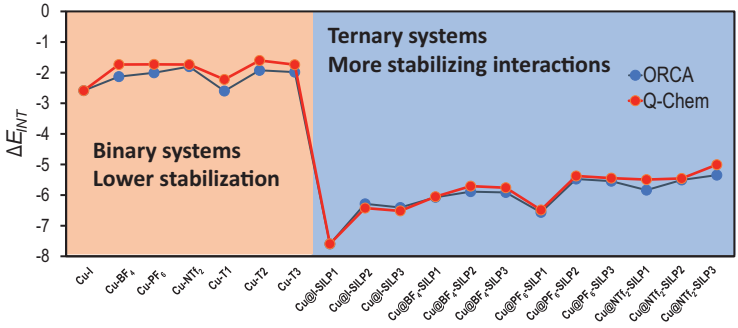

Fig. 2. Comparative plot trends of the interaction energy calculated using ORCA and Q-Chem for the binary and ternary systems based on the Cu@(X)SILPs, where $X = I$, BF_4, PF_6, and NTf_2. Modified from [1].

The thermodynamic function can be calculated from full relaxed structures based on the vibrational analysis. This analysis is carried out considering the pressure of 1 atm and temperature of 298.15 K. The thermodynamic functions ΔG, ΔH, and TΔS were calculated for the adsorption process, according to $\Delta G_{ads} = \Delta H_{ads} - T\Delta S_{ads}$. The thermodynamic functions indicate that reaction occurs spontaneously ($\Delta G_{ads} < 0$) thanks to enthalpic contributions since the thermoentropic function does not support the spontaneity of the reaction showing positive values of $-T\Delta S_{ads}$.

From the thermodynamic statistic point of view, each parameter can be divided according to the partition function. Thus, $U = U_{elec} + ZPE + U_{vib} + U_{rot} + U_{trans}$, where U_{elec} is the electron energy, *ZPE* is the zero-point energy, U_{vib} is the vibrational inner energy, U_{rot} is the rotational inner energy, and U_{trans} is the translational energy. Then, enthalpy is expressed as $H = U + H_{corr}$; H_{corr} is the thermal correction to enthalpy. The entropy is also divided by the partition function in the following parts: $S = S_{elec} + S_{vib} + S_{rot} + S_{trans}$, where S_{elec}, S_{vib}, S_{rot}, and S_{trans} are the electronic, vibrational, rotational, and translation entropy terms, being $S_{elec} = 0$ because there is no change in the multiplicity during the adsorption reaction. Thus, considering that the partition function was decomposed thermodynamically, the different contributions can affect the adsorption's spontaneity. Fig. 3 summarizes the percentual contributions of each partition function for the studied thermodynamic functions. The endergonic contribution ($\Delta G > 0$) decreases the spontaneity, while the exergonic contributions ($\Delta G < 0$), support the spontaneity of the adsorption reaction. Exergonic contributions correspond to ΔU_{elec}, ΔZPE, ΔU_{rot}, ΔU_{trans}, H_{corr}, and $-T\Delta S_{vib}$, and the endergonic contribution correspond to ΔU_{vib}, $-T\Delta S_{rot}$, and $-T\Delta S_{trans}$. The exergonic component is dominated by the $\Delta U_{elec,}$ which is the Eads negative, while for endergonic contribution is $-T\Delta S_{trans}$ (Fig. 3a). Interestingly, the exergonic adsorption process showed a higher contribution of ΔU_{elec} for the anion complexes, where the Cu-I^- complex presents 90% of ΔU_{elec}, while the Cu-PF_6^- and Cu-NTf_2^- complexes showed contributions of 75% of ΔU_{elec}. Another exergonic contribution corresponds to the increase of vibrational entropy showing the highest value for Cu-NTf_2^- complex (18%) and the lowest for Cu-I^- (7%). For the endergonic terms, Cu-I^- complex exhibits the highest contribution of 98%, associated with a decreasing of the translation entropy, whereas the Cu-NTf_2^- complex shows the lowest contribution reaching 49%.

For cations, the highest exergonic contribution was observed by the ΔU_{elec} term in the Cu-$T1^+$ complex with 62%, while the lowest value was 54% for Cu-$T3^+$. The endergonic contribution of each cation has the same contributions for ΔU_{vib}, $-T\Delta S_{rot}$, and $-T\Delta S_{trans}$ with values of 14, 38, and 48%, respectively. For the Cu@(X)SILP complexes, the ΔU_{elec} and $-T\Delta S_{vib,}$ are the most critical terms, where the values are ranged between 80 and 87% and 8–13%, respectively. A similar landscape is observed for an endergonic term where the $T\Delta S_{rot}$, and $-T\Delta S_{trans}$ displays higher contributions with values of 26–38% and 49–65%, respectively.

The detailed information of the carried about thermodynamic analyses can be revised in the attached data linked to this work (files "Thermodynamic-decomposition-Analysis-CuSILP.xlsx" and "Thermodynamic-functions-cusilp.xlsx"). Formulas and values are included in the cited files.

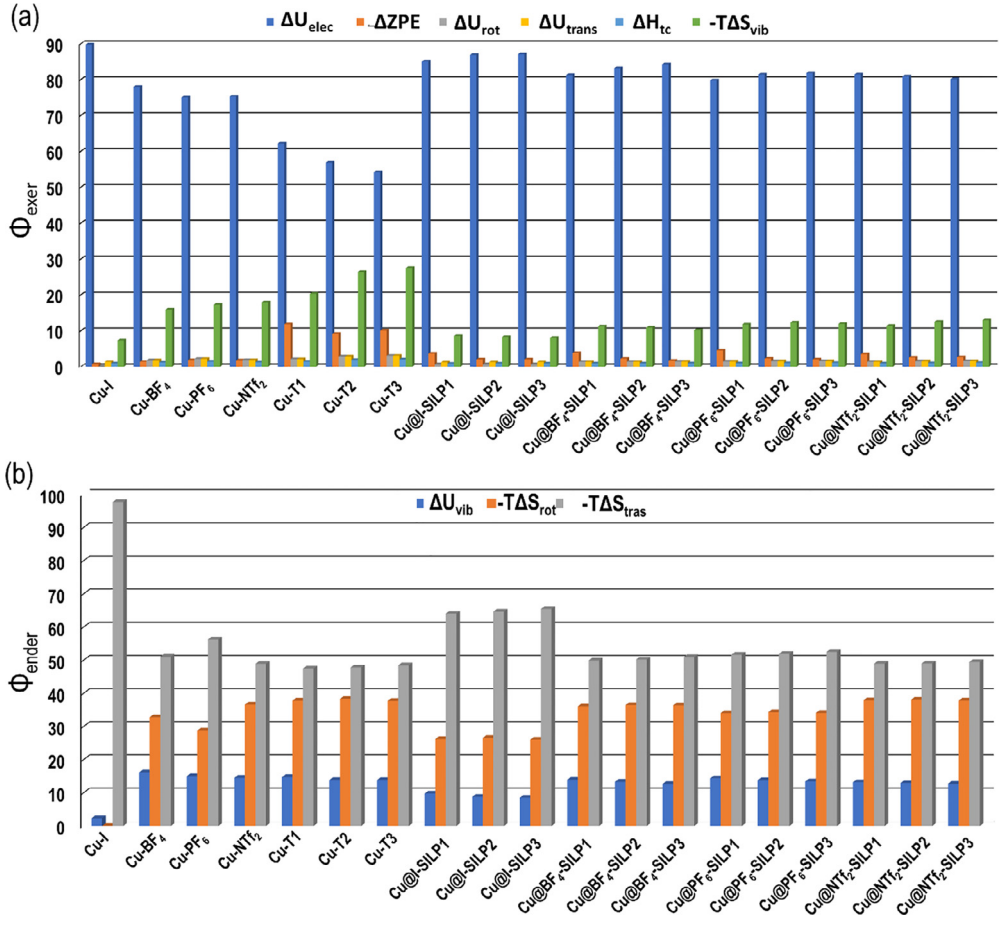

Fig. 3. Percentual (a) exergonic contributions (Φ_{exer}) and (b) endergonic contributions (Φ_{ender}) for the binary and ternary systems based on the Cu@(X)SILPs, where $X = I$, BF_4, PF_6, and NTf_2.

The structural analysis of the intermolecular interaction of Cu-anion, Cu-cation, and Cu@SILP1–3 complexes can be described using Atom in Molecules analysis evaluating the electron density at the bond critical points (BCPs). The atom in molecules (AIM) studies were developed considering the following critical point searching parameter: Maximal iterations of 1000; a scale factor of step-size of 0.50; criteria for electron density gradient-norm convergence of 1.0×10^{-6}; criteria for displacement convergence: 1.0×10^{-7}; minimal distance between Critical Points of 0.03 Bohr. Skip search if the distance between atoms is longer than the sum of their van der Waals radius multiplied by 1.80; and the criteria for determining if the Hessian matrix is singular of 1.0×10^{-50}. Detailed information for the AIM evaluation can be checked in the data set included in this article; specifically, in the directory AIM-Summary. The files can be visualized with any text editor; however, the authors recommend Geany and content some modifications to obtain the Poincare-Hopf condition required for these analyses (DOI: http://dx.doi.org/10.17632/zr3vf3bxpk.1).

The donor-acceptor interactions were evaluated using the fragmental charges (Δq). Fig. 4 summarized the obtained results for the complex fragments, including Cu_{55}, anions, and cations. Detailed information about the fragmental charge calculation can be revisited in the fragmental-Charge-CM5.xlsx file included in the Data set of these articles. The file can be used as payroll for other studies since it contains the formulae for the fragment calculation.

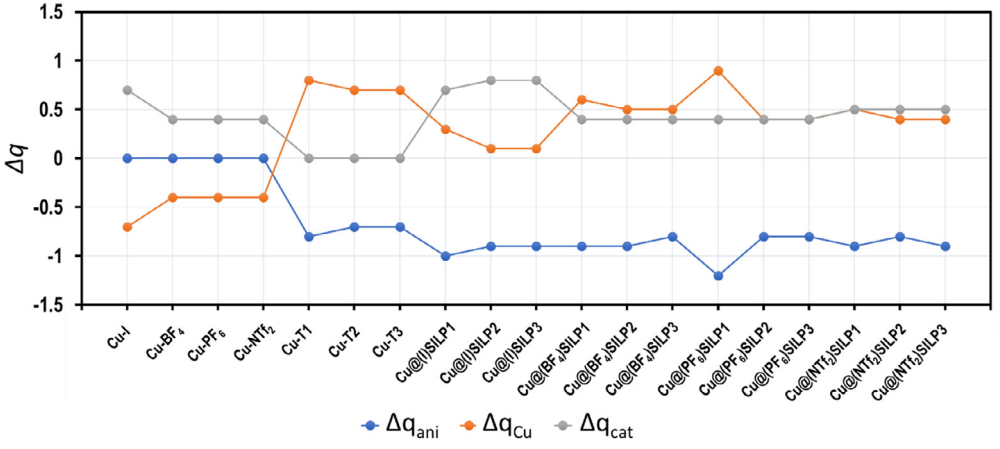

Fig. 4. Plot of fragmental charges employing the population model CM5 developed by Truhlar for the binary and ternary systems based on the Cu@(X)SILPs, where $X = I$, BF_4, PF_6, and NTf_2.

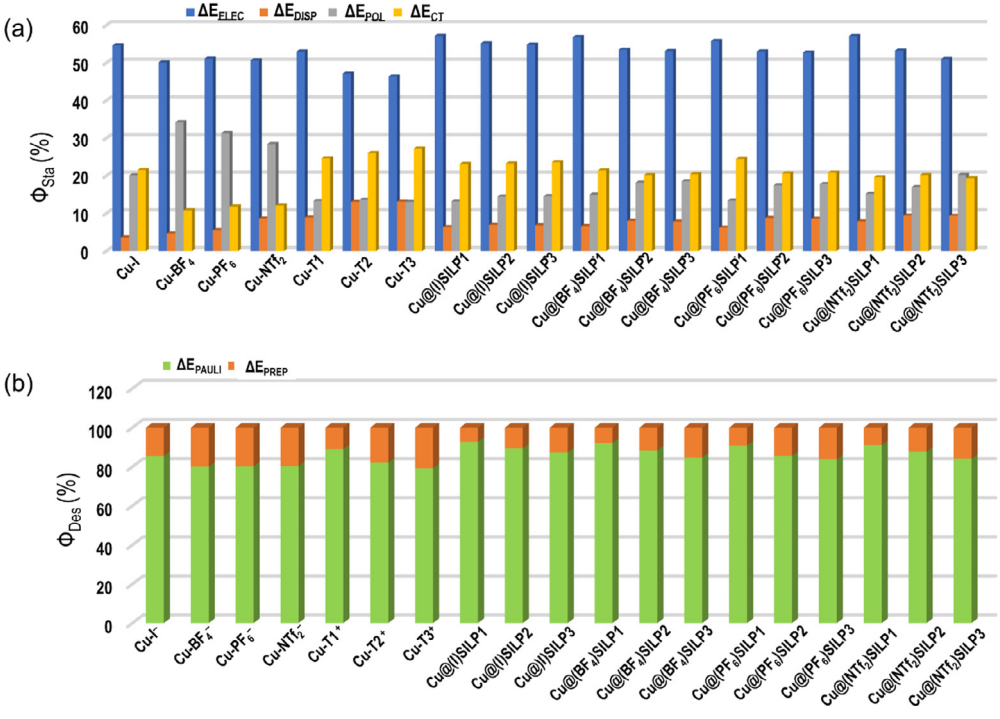

Fig. 5. Relative percentual contributions to the (a) stabilizing and (b) destabilizing energy binary and ternary systems based on the Cu@(X)SILPs, where $X = I$, BF_4, PF_6, and NTf_2. Calculations based on ALMO-EDA method.

The ALMO-EDA results for stabilizing and destabilizing terms are presented (Fig. 5). The destabilizing terms for the studied complexes are displayed graphically in Fig. 5b, showing the dominance of ΔE_{PAULI} in destabilizing terms.

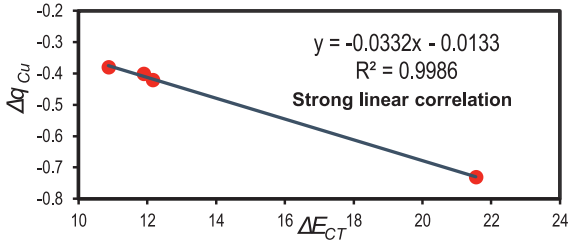

Fig. 6. Plot Δq_{Cu} vs ΔE_{CT} for anionic binary systems: Cu-I^-, Cu-BF_4^-, Cu-PF_6^-, and Cu-NTf_2^-. Linear correlation is described inset. Modified from [1].

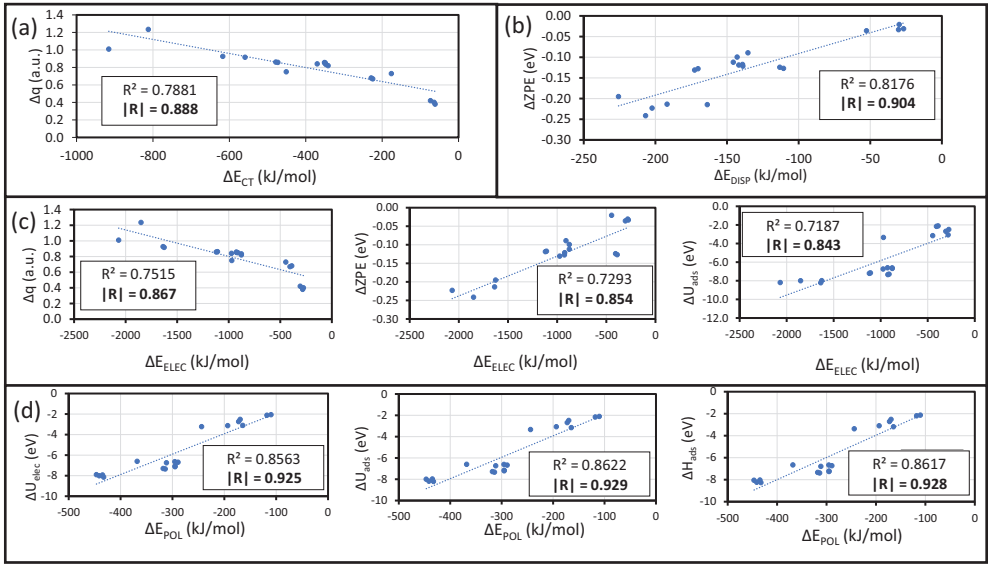

Fig. 7. Correlation plot for the (a) ΔE_{CT}, (b) ΔE_{DISP}, (c) ΔE_{ELEC}, and (d) ΔE_{POL} stabilizing terms. Modified from [1].

For the anionic complexes, the correlation between Δq_{Cu} and ΔE_{CT} is presented in Fig. 6, where it is possible to observe that fragmental charge is linearly correlated to charge transfer energy.

Other properties are related to the energy decomposition by the ALMO-EDA method. A correlation analysis was carried to calculate the following properties: ionization potential (IP), electron affinity (EA), electronic chemical potential (μ), electron hardness (η), electrophilicity (ω), dipolar moment (δ), maximum electron transfer (Δq), and the thermodynamic properties obtained from vibrational analysis such as ΔU_{ads}, ΔH_{ads}, $-T\Delta S_{ads}$, ΔG_{ads} including its electronic, vibrational, rotational and translational contributions. For this purpose, the statistical analysis was developed using the linear regression procedure using an Excel program. The correlation plots are displayed in (Fig. 7). In the case of ΔE_{CT}, the higher correlation parameter is Δq, which is intrinsically related to the charge transfer phenomena and the electron flow between fragments (Fig. 7a). Secondly, ΔE_{DISP} presents several high contributions, but the more correlated is the ΔZPE with a value of 0.904 (Fig. 7b). However, other significant contributions are those related to δ since dispersion interaction also occurs from low weak electrostatic interaction with dipoles. For ΔE_{ELEC}, the stronger correlations are Δq, ΔZPE, and ΔU_{tot} with values of 0.867, 0.854, and 0.843 (Fig. 7c), respectively. This behavior can be explained, considering that the electron transfer contributes to the permanent coulombic interactions since Cu_{55} turns on a charged fragment

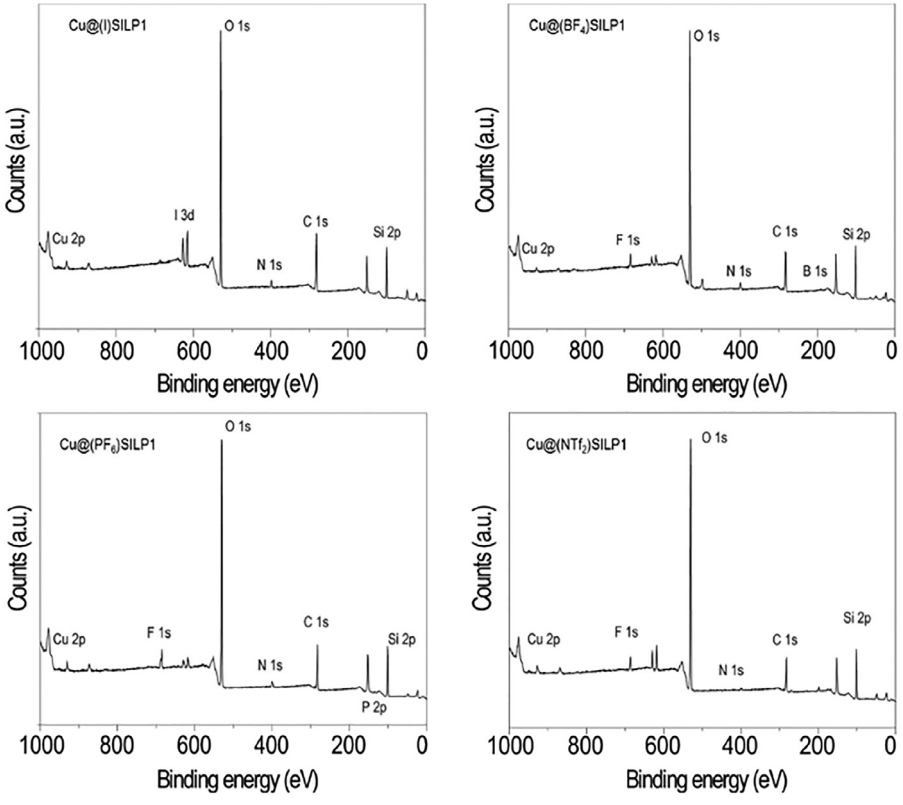

Fig. 8. Wide range XPS spectra of Cu@(I)SILP1, Cu@(BF_4)SILP1, Cu@(PF_6)SILP1, and Cu@(NTf_2)SILP1. Modified from [1].

that interacts with both anion and cation. The ΔZPE and ΔU_{tot} are relevant terms in the electronic energy of reaction, having a close relation to the higher contribution of ΔE_{ELEC}. Finally, ΔE_{POL}, the thermodynamic parameter without BSSE corrections (Fig. 7d), that is, ΔU_{elec}, ΔU_{ads}, and ΔH_{ads} display strong correlations with 0.925, 0.929 and 0.928, respectively. The mentioned thermodynamic functions contain the stabilization energy mainly ΔU_{elec} as a higher contribution indicating that the internal electronic contribution is intrinsically involved in polarization phenomena. Correlation analyses of all the before mentioned properties are displayed in the file "Correlation-Data.xlsx"; the detailed information of the correlation factor method and subsequent analysis are incorporated in the Data Set.

Fig. 8 displays the XPS spectra of the Cu@SILP1 complexes with the respective anions.

Detailed information of the XPS spectra and raw spectra can be found in the file called "RAw Data in brief.opj" included in the Data Set attached to this work.

2. Experimental Design, Materials and Methods

2.1. Materials

Iodobenzene, 3-iodopropyltrimethoxysilane, benzyl bromide, phenylacetylene, NaN_3, $CuCl_2 \times 2H_2O$, CuI, $NaBH_4$, $MgSO_4$, $NaBF_4$, KPF_6, and $LiNTf_2$, and $BMI.BF_4$ were purchased from Sigma Aldrich. All chemicals were used without further purification, except for DCM, toluene, MeOH, acetonitrile, Et_2O, and EtOAc, which were purified by standard procedures [6].

2.2. Synthesis of 1,2,3-Triazolium derivatives

Alkyne (5 mmol, 1.0 eq.), alkyl halide (1.0 eq.), and NaN_3 (1.3 eq.) were loaded into a 25 mL round-bottom flask. Then [$CuI(PPh_3)_3$] (0.05 mol%) was added and dissolved in water (5 mL). The reaction was stirred for 4 h at room temperature, and the progress of the reaction was monitored using thin-layer chromatography (TLC). After its completion, the reaction mixture was filtered, and the residue was dissolved in DCM. The combined organic layer was later concentrated in a vacuum to yield the corresponding triazoles.

2.3. Synthesis of SILP(X) 1–3

SiO_2–I (5 g) was suspended in dry acetonitrile (30 mL), with stoichiometric amounts of triazoles1–3 and refluxed during 24 h. Then, the particles were collected by filtration and repeatedly washed with petroleum ether, and then dried off under vacuum at 110 °C for 4 h to obtain SILP1–3 powder. Based on the amount of IL on the SILP(I)1–3 supports, an excess (1.2 eq.) of $NaBF_4$, KPF_6, and $LiNTf_2$ salts were dissolved in deionized water (25 mL) and added to the SILP(I)1–3 (1.0 g) in order to exchange the anions. The suspensions were vigorously stirred for 48 h. The mixtures were washed, centrifuged, and dried to yield the supports SILP(BF_4)1–3, SILP(PF_6)1–3, and SILP(NTf_2)1–3.

2.4. Synthesis of SiO_2-I

Initially, 200 g mesh silica gel was soaked in 30% HCl overnight to hydrolyze its surface. Next, activated silica gel (100 g) was suspended in dry toluene (30 mL) in a round-bottom flask equipped with a reflux condenser under nitrogen. While being stirred, 3-iodopropyltrimethoxysilane (0.05 M) was added dropwise. The suspension was refluxed for 72 h. After cooling, the solid was collected by filtration and exhaustively washed by Soxhlet extraction with ethanol and water, and then dried under reduced pressure to yield iodopropyl–silica gel (SiO_2–I).

2.5. Synthesis of Cu@(x)SILP1–3

A solution of $CuCl_2 \times 2H_2O$ (0.25 mmol) and MeOH (20 mL) was added to SILP(X)1–3 (100 mg) under constant stirring at room temperature for 30 min. A solution of $NaBH_4$ (5 mmol) dissolved in MeOH (3 mL) was added to the reaction mixture dropwise. The reaction mixture turned black due to the formation of Cu NPs that were washed with MeOH (3×10 mL) and Et_2O (3×10 mL). Subsequently, the samples were isolated by centrifugation (4500 rpm) and dried under reduced pressure.

2.6. X-ray photoelectron spectroscopy

XPS Experiment was collected by powder sample that was mounted on double-sided tape (Sellotape) and pressed to ensure proper coverage of the tape with the powder. X-ray Photoelectron Spectroscopy (XPS) measurements were performed using a Kratos AXIS Ultra DLD instrument. The chamber pressure during the measurements was 5×10^{-9} Torr. Wide energy range survey scans were collected at pass energy of 80 eV in hybrid slot lens mode and a step size of 0.5 eV. High-resolution data on the C 1 s, N 1 s, and F 1 s photoelectron peaks were collected at pass energy 20 eV over energy ranges suitable for each peak, and collection times of 5 min, step sizes of 0.1 eV. The charge neutralizer filament was used to prevent the sample from charging over the irradiated area. The X-ray source was a monochromated Al K_α emission, run at 10 mA and 12 kV (120 W). The energy range for each 'pass energy' (resolution) was calibrated using the

Kratos Cu $2p_{3/2}$, Ag $3d_{5/2}$, and Au $4f_{7/2}$ three-point calibration method. The data were charge corrected to the reference carbon adventitious signal at 284.8 eV. The transmission function was calibrated using a clean gold sample method for all lens modes and the Kratos transmission generator software within Vision II. The data were processed with CASAXPS (Version 2.3.17).

2.7. ALMO-EDA calculations

Calculations were calculated using Q-Chem 5.2 computational package [3,4]. For energy decomposition analysis based on absolutely localized molecular orbitals (ALMO-EDA), the following parameters were considered: Self-consistent Field algorithm corresponds to a mixture of DIIS and Geometrical Direct Minimization using an energy convergence criterion of 1×10^{-6} Hartree with no symmetry restriction. Stoll Fragmentation method employing Roothaan-step and exact SCF correction methods after the locally-projected equations. The basis set superposition error (BSSE) and dispersion D3BJ corrections were included.

2.8. AIM analysis

The atom in molecules studies (AIM) were developed using the Multiwfn3.6 program [7] and its routine of Topology analysis (option 2). These calculations were carried out considering the following critical point searching parameter: Maximal iterations of 1000; a scale factor of step-size of 0.50; criteria for electron density gradient-norm convergence of 1.0×10^{-6}; criteria for displacement convergence: 1.0×10^{-7}; minimal distance between Critical Points of 0.03 Bohr. Skip search if the distance between atoms is longer than the sum of their van der Waals radius multiplied by 1.80; and the criteria for determining if the Hessian matrix is singular of 1.0×10^{-50}.

2.9. Fragmental charge calculation

Fragmental charges were calculated using the Charge Model 5 population analysis [8], which is implemented in the Multiwfn3.6 program [7] in the routine of population analysis and atomic charges (option 7).

CRediT Author Statement

Kerry Wrighton-Araneda: Conceptualization, Formal analysis, Investigation, Methodology, Software, Validation, Visualization, Writing - original draft, Writing - review & editing. **Cristián Valdebenito:** Investigation, Writing - original draft, Visualization, Validation. **Gabriel Abarca:** Investigation, Conceptualization, Funding acquisition, Investigation, Methodology, Project administration, Resources, Software, Supervision, Writing - review & editing, Data curation. **Diego Cortés-Arriagada:** Investigation, Conceptualization, Funding acquisition, Investigation, Methodology, Project administration, Resources, Software, Supervision, Writing - review & editing, Data curation.

Declaration of Competing Interest

The authors declare that they have no known competing for financial interests or personal relationships which have, or could be perceived to have, influenced the work reported in this article.

Acknowledgments

D.C-A thanks the financial support of the CONICYT/FONDECYT project #11170289 and the computational resources through the CONICYT/FONDEQUIP project EQM180180. Project supported by the Fund of Scientific and Technological Equipment, year 2018, code L318-04, Universidad Tecnológica Metropolitana. Powered@NLHPC: This research was partially supported by the supercomputing infrastructure of the NLHPC (ECM-02). K.W-A acknowledges the financial support of CONICYT/FONDECYT de Postdoctorado #3200270. G.A thanks FONDECYT Iniciación 11170879 and Project Anillo ACT192175.

References

[1] K. Wrighton-Araneda, C. Valdebenito, M.B. Camarada, G. Abarca, D. Cortés-Arriagada, Interaction of supported ionic liquids phases onto copper nanoparticles: a DFT study, J. Mol. Liq. 310 (2020) 113089 https://doi.org/10.1016/j.molliq.2020.113089.

[2] S.F. Boys, F. Bernardi, The calculation of small molecular interactions by the differences of separate total energies. Some procedures with reduced errors, Mol. Phys. 19 (1970) 553–566 https://doi.org/10.1080/00268977000101561.

[3] A.I. Krylov, P.M.W. Gill, Q-Chem: an engine for innovation, Wiley Inter-discipline, Rev. Comput. Mol. Sci. 3 (2013) 317–326 https://doi.org/10.1002/wcms.1122.

[4] Y. Shao, Z. Gan, E. Epifanovsky, A.T.B. Gilbert, M. Wormit, J. Kussmann, A.W. Lange, A. Behn, J. Deng, X. Feng, D. Ghosh, M. Goldey, P.R. Horn, L.D. Jacobson, I. Kaliman, R.Z. Khaliullin, T. Kuś, A. Landau, J. Liu, E.I. Proynov, Y.M. Rhee, R.M. Richard, M.A. Rohrdanz, R.P. Steele, E.J. Sundstrom, H.L. Woodcock, P.M. Zimmerman, D. Zuev, B. Albrecht, E. Alguire, B. Austin, G.J.O. Beran, Y.A. Bernard, E. Berquist, K. Brandhorst, K.B. Bravaya, S.T. Brown, D. Casanova, C.-.M. Chang, Y. Chen, S.H. Chien, K.D. Closser, D.L. Crittenden, M. Diedenhofen, R.A. DiStasio, H. Do, A.D. Dutoi, R.G. Edgar, S. Fatehi, L. Fusti-Molnar, A. Ghysels, A. Golubeva-Zadorozhnaya, J. Gomes, M.W.D. Hanson-Heine, P.H.P. Harbach, A.W. Hauser, E.G. Hohenstein, Z.C. Holden, T.-.C. Jagau, H. Ji, B. Kaduk, K. Khistyaev, J. Kim, J. Kim, R.A. King, P. Klunzinger, D. Kosenkov, T. Kowalczyk, C.M. Krauter, K.U. Lao, A.D. Laurent, K.V. Lawler, S.V. Levchenko, C.Y. Lin, F. Liu, E. Livshits, R.C. Lochan, A. Luenser, P. Manohar, S.F. Manzer, S.-.P. Mao, N. Mardirossian, A.V. Marenich, S.A. Maurer, N.J. Mayhall, E. Neuscamman, C.M. Oana, R. Olivares-Amaya, D.P. O'Neill, J.A. Parkhill, T.M. Perrine, R. Peverati, A. Prociuk, D.R. Rehn, E. Rosta, N.J. Russ, S.M. Sharada, S. Sharma, D.W. Small, A. Sodt, T. Stein, D. Stück, Y.-.C. Su, A.J.W. Thom, T. Tsuchimochi, V. Vanovschi, L. Vogt, O. Vydrov, T. Wang, M.A. Watson, J. Wenzel, A. White, C.F. Williams, J. Yang, S. Yeganeh, S.R. Yost, Z.-.Q. You, I.Y. Zhang, X. Zhang, Y. Zhao, B.R. Brooks, G.K.L. Chan, D.M. Chipman, C.J. Cramer, W.A. Goddard, M.S. Gordon, W.J. Hehre, A. Klamt, H.F. Schaefer, M.W. Schmidt, C.D. Sherrill, D.G. Truhlar, A. Warshel, X. Xu, A. Aspuru-Guzik, R. Baer, A.T. Bell, N.A. Besley, J.-.D. Chai, A. Dreuw, B.D. Dunietz, T.R. Furlani, S.R. Gwaltney, C.-.P. Hsu, Y. Jung, J. Kong, D.S. Lambrecht, W. Liang, C. Ochsenfeld, V.A. Rassolov, L.V. Slipchenko, J.E. Subotnik, T. Van Voorhis, J.M. Herbert, A.I. Krylov, P.M.W. Gill, M. Head-Gordon, Advances in molecular quantum chemistry contained in the Q-Chem 4 program package, Mol. Phys. 113 (2015) 184–215 https://doi.org/10.1080/00268976.2014.952696.

[5] D.S. Levine, M. Head-Gordon, Energy decomposition analysis of single bonds within Kohn-Sham density functional theory, Proc. Natl. Acad. Sci. 114 (2017) 12649–12656 https://doi.org/10.1073/pnas.1715763114.

[6] W.L.F. Armarego, Purification of laboratory chemicals, (2017). http://app.knovel.com/hotlink/toc/id:kpPLCE0062/purification-of-laboratory.

[7] T. Lu, F. Chen, Multiwfn: a multifunctional wavefunction analyzer, J. Comput. Chem. 33 (2012) 580–592 https://doi.org/10.1002/jcc.22885.

[8] A.V. Marenich, S.V. Jerome, C.J. Cramer, D.G. Truhlar, Charge model 5: an extension of hirshfeld population analysis for the accurate description of molecular interactions in gaseous and condensed phases, J. Chem. Theory Comput. 8 (2012) 527–541 https://doi.org/10.1021/ct200866d.